Effects of Molecular Structure on Phase Transitions of Ionic Plastic Crystals Containing Cationic Sandwich Complexes

Kimata, Hironori

Mochida, Tomoyuki

(Citation)
Crystal Growth & Design,18(12):7562-7569

(Issue Date)
2018-12-05

(Resource Type)
journal article

(Version)
Accepted Manuscript

Effects of Molecular Structure on Phase Transitions of Ionic Plastic Crystals Containing Cationic Sandwich Complexes

Hironori Kimata and Tomoyuki Mochida*

Department of Chemistry, Graduate School of Science, Kobe University, Rokkodai, Nada, Hyogo 657-8501, Japan. E-mail: tmochida@platinum.kobe-u.ac.jp

Keywords: Plastic crystals, sandwich complexes, organometallic compounds, phase transitions, crystal structures, thermal properties

ABSTRACT: Salts of sandwich complexes often exhibit a plastic phase at high temperatures. To determine a molecular design that can achieve a plastic phase at lower temperatures, we synthesized $[CoCp_2][X]$ and $[Ru(Cp)(C_6H_6)][X]$ (Cp = C_5H_5) with various anions (X = monocarba-*closo*-dodecaborate ($CB_{11}H_{12}^-$), $B(CN)_4^-$, $CF_3BF_3^-$, OTf^-, BF_4^-, $C(CN)_3^-$, and tris(pentafluoroethyl)trifluorophosphate (FAP^-)) and investigated their phase behaviors. All of the salts except the $C(CN)_3$ and FAP salts exhibited a plastic phase. The phase transition temperature to the plastic phase tended to decrease with decreasing anion size. This tendency contrasts that observed in octamethyl- and decamethylferrocenium salts. Although the phase transition temperatures of most salts were high, those of $[CoCp_2][CF_3BF_3]$, $[Ru(Cp)(C_6H_6)][CF_3BF_3]$, and $[Ru(Cp)(C_6H_6)][BF_4]$ were below 300 K. The plastic phases of the salts had a CsCl-type structure. Crystal structure determinations at low temperatures revealed that the cations and anions were arranged alternately in most of the salts. However, the $C(CN)_3$ salts exhibited a stacking arrangement of the cations, which is responsible for the absence of a plastic phase.

INTRODUCTION

In recent years, ionic plastic crystals have attracted much attention because of their ionic conductivities, electronic properties, and phase transition phenomena.[1–14] A plastic phase is exhibited by solids composed of globular molecules that can undergo rotational motion in the crystal. Plastic crystals have highly symmetric crystal lattices, such as cubic or hexagonal, and their melting entropies are small owing to the orientational disorder of the molecules.[15,16] The majority of plastic ionic crystals are onium salts, many of which are closely related to ionic liquids in terms of molecular structure. Although many ionic plastic crystals have been reported thus far, the crystal engineering factors that affect the phase transition temperature to the plastic phase are not well understood.

Recently, we developed organometallic ionic plastic crystals[17-20] and ionic liquids[21-24] containing cationic sandwich complexes and elucidated their boundary in terms of molecular shape.[21-23] Considering the unique properties of metallocenes, such as their magnetism and reactivities, we expect that exploration of organometallic compounds will expand the science base and applications of molecular ionic materials. Salts of simple sandwich complexes have been known to exhibit plastic phases.[25-28] For example, $[FeCp_2][PF_6]$,[8] $[CoCp_2][PF_6]$,[25] and $[RuCp(C_6H_6)][PF_6]$[27] (Cp = C_5H_5) exhibit a phase transition to the plastic phase at 347 K, 314 K, and 333 K, respectively. However, the phase transition temperatures of organometallic plastic crystals are generally much higher than those of onium salts, making them less suitable for the investigation of physical phenomena and applications. Only a few salts with a phase transition temperature below 300 K are known.[18,20]

Based on these backgrounds, we aimed to elucidate the factors that govern the phase transition temperature of organometallic ionic plastic crystals and to search for a material design that can achive lower transition temperature. We have previously demonstrated that the transition temperature in the salts of octamethyl- and decamethylferrocenium cations decreases with increasing anion size.[17,18] In this study, to investigate the effect of cation size, we synthesized

[$CoCp_2$][X] ([**1**][X]) and [$RuCp(C_6H_6)$][X] ([**2**][X]) containing smaller cations (Figure 1). A variety of anions were used, including monocarba-*closo*-dodecaborate ($CB_{11}H_{12}^-$), $CF_3BF_3^-$, $CF_3SO_3^-$ (OTf^-), BF_4^-, $B(CN)_4^-$, $C(CN)_3^-$, and tris(pentafluoroethyl)trifluorophosphate (FAP). $CB_{11}H_{12}^-$ is a large spherical anion with a volume (179 $Å^3$) comparable with that of the cation ($[\mathbf{1}]^+$: 167 $Å^3$, $[\mathbf{2}]^+$: 187 $Å^3$). The crystal structures of its alkylferrocenium salts have been reported.[29] The CF_3BF_3 anion has been known to produce ionic liquids and ionic plastic crystals.[30,31] OTf^- and $CF_3BF_3^-$ have nearly identical shapes and volumes (85 and 84 $Å^3$, respectively); hence, they are suitable for investigating the effect of the charge distribution in the anion. FAP is a non-spherical anion, with a much larger volume (244 $Å^3$) than the cations used.

In this paper, we discuss the thermal properties and crystal structures of these salts, focusing on their phase transition to the plastic phase. The thermal properties and crystal structures of [**2**][$B(CN)_4$] and [**2**][$C(CN)_3$] have been reported previously.[20] The crystal structures of [**1**][OTf][32] and [**1**][BF_4] are known.[33] This study shows that CF_3BF_3 is a useful anion that exhibits the plastic phase at low temperatures, whereas $CB_{11}H_{12}^-$ has a very high phase transition temperature, despite its spherical shape. Furthermore, the dependence of the transition temperature on the anion size was found to be opposite to that observed in octamethyl- and decamethylferrocenium salts, which is probably attributable to their structural differences.

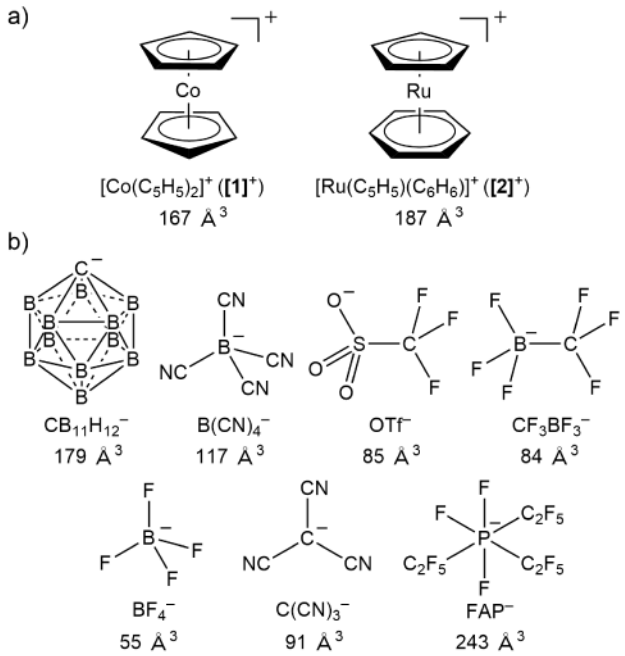

Figure 1. Structural formulae of (a) cationic sandwich complexes and (b) anions used in this study. The van der Waals volumes of these molecules, estimated by density functional theory calculations, are shown below.

RESULTS AND DISCUSSION

Phase behavior. We synthesized [**1**][X] and [**2**][X] through anion exchange using the corresponding chloride salts and carried out differential scanning calorimetry (DSC) measurements. The phase diagrams and DSC curves of the salts are shown in Figure 2 and Figure S1 (Supporting Information), respectively. As seen from the phase diagram, the phase behaviors of [**1**][X] and [**2**][X] were approximately similar. All salts except the $C(CN)_3$ and FAP salts exhibited a plastic phase. The phase transition temperatures of the CF_3BF_3 salts and [**2**][BF_4] were below 300 K. The $C(CN)_3$ and FAP salts melted at high temperatures without exhibiting a plastic phase.

The transition temperature (T_C) of [**1**][X] to the plastic phase generally decreased with decreasing anion volume ($CB_{11}H_{12}$ > $B(CN)_4$ > OTf ≈ CF_3BF_3; 402.1 K–277.2 K), whereas the transition temperature of [**1**][BF_4] (T_c = 418.4 K) was very high. [**2**][X] showed a trend approximately similar to [**1**][X], although the transition temperatures of the $CB_{11}H_{12}$ and BF_4 salts differed from those of the corresponding [**1**][X] salts by more than 100 K. Interestingly, the transition temperatures of the $CB_{11}H_{12}$ salts were very high, despite their spherical anions (402.1 and 500.8 K). It is noteworthy that the transition temperatures of [**1**][CF_3BF_3] (T_C = 277 K), [**2**][CF_3BF_3] (T_C = 267.2 K), and [**2**][BF_4] (T_C = 293.2 K) were below 300 K. The transition temperatures of the CF_3BF_3 salts were lower than those of the corresponding OTf salts by approximately 90 K, despite their comparable anion sizes. These transition temperatures are lower than those of the other sandwich complex salts reported to date, demonstrating that CF_3BF_3 is a useful anion for lowering the transition temperature. The negative charge of $CF_3BF_3^-$ resides on the B atom, having a smaller Coulombic interaction with the cation than OTf^-, which probably led to the low transition temperature.

On the other hand, the $C(CN)_3$ and FAP salts did not exhibit a plastic phase. This is ascribed to the crystal structure of the $C(CN)_3$ salts having no alternate arrangement of the ions (see below) and to the large deviation of the FAP anion from the spherical shape (ovality = 1.40) compared with other anions (ovality = 1.12–1.23). These salts exhibited a liquid phase instead of a plastic phase at high temperatures (T_m = 363–446 K; ΔS_m = 28–37 J mol^{-1} K^{-1}).

Most of these salts exhibited a solid-phase transition at a lower temperature than the phase transition to the plastic phase or melting, which is probably due to the successive enhancement of the motions of the anions and cations. Salts of sandwich complexes often exhibit such successive phase transitions.[17] The phase transition in [**1**][$CB_{11}H_{12}$] from phase I to phase II was examined crystallographically (see below). The sums of the solid-phase transition entropies in [**2**][X] were larger than those in [**1**][X] by 4–19 JK^{-1}mol^{-1}, except for the CF_3BF_3 and FAP salts, which is probably ascribable to the less-symmetric structure of the cation.

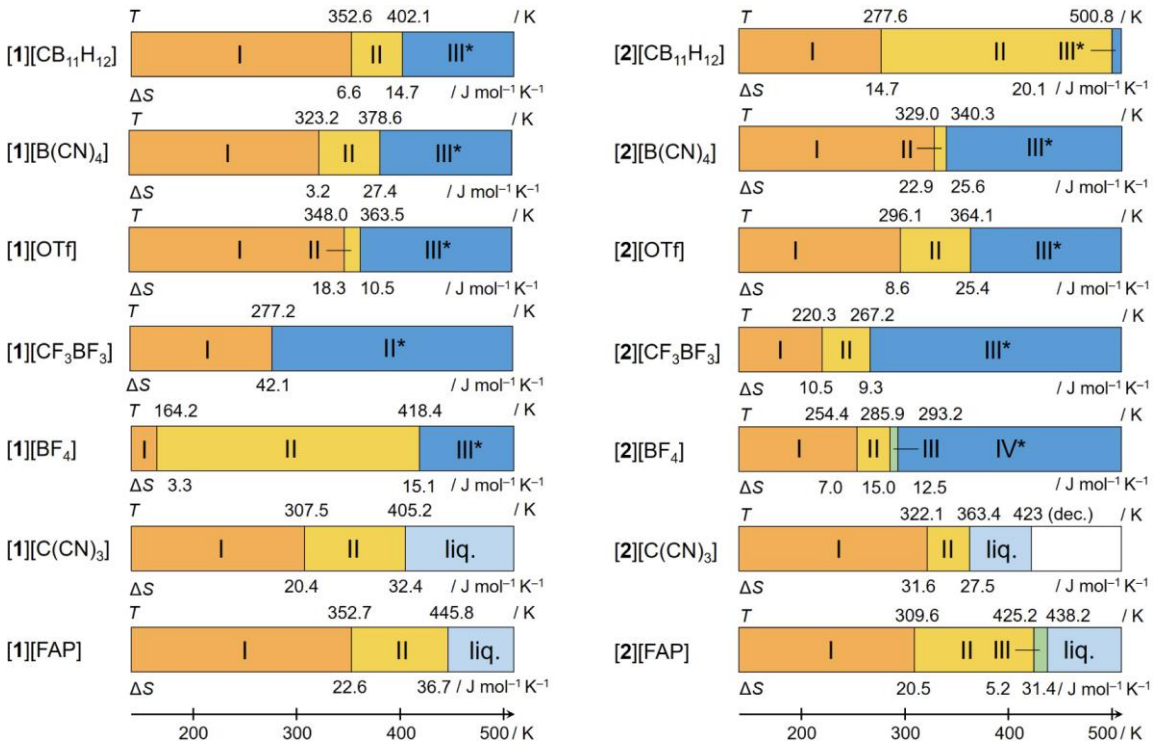

Figure 2. Phase diagrams of [**1**][X] and [**2**][X] (X = $CB_{11}H_{12}$, $B(CN)_4$, OTf, CF_3BF_3, $C(CN)_3$, FAP). The phase transition temperature (K) and the phase transition entropy (J mol^{-1} K^{-1}) are shown above and below each bar chart, respectively. The asterisks represent plastic phases. Data for [**2**][X]

($X = B(CN)_4$ and $C(CN)_3$) were taken from Ref. 20.

Structures of the plastic phase. Powder X-ray diffraction analysis revealed that the plastic phases of these salts have a CsCl-type structure. The X-ray diffraction (XRD) patterns are shown in Figure S2 (Supporting Information) and the lattice constants and interionic distances derived from the data are shown in Table 1. The radii of $[\mathbf{1}]^+$ and $[\mathbf{2}]^+$, calculated from the van der Waals volumes and assuming the molecule to be a sphere, were 3.42 and 3.55 Å, respectively, whereas the radii of $B(CN)_4^-$, OTf^-, $CF_3BF_3^-$, and BF_4^- were 3.04, 2.73, 2.71, and 2.36 Å, respectively. The interionic distances were found to be comparable to the sum of the ionic radii (Table 1). The coordination number was eight, which was identical to the coordination number in the low-temperature phase (Phase I; see below). According to the radius ratio rule for inorganic ionic crystals,[34] a salt with a radius ratio ($\rho = r_{\text{small ion}}/r_{\text{large ion}}$) greater than 0.73 exhibits a CsCl-type structure with coordination number eight, whereas a salt with a radius ratio between 0.41–0.73 exhibits a NaCl- or NiAs-type structure with coordination number six. Most of the radius ratios of the studied salts are greater than 0.73 (Table 1), and hence the structures are in agreement with the radius ratio rule. However, [**1**][BF_4] ($\rho = 0.69$) and [**2**][BF_4] ($\rho = 0.66$) have a CsCl-type structure although their radius ratios are smaller than 0.73. This is probably owing to the non-spherical shape of the ions and the softness of molecular ionic crystals. We have previously reported that the plastic phase of $[Fe(C_5Me_4H)_2][X]$ ($X = B(CN)_4$, $C(CN)_3$, and $FeCl_4$; $\rho < 0.72$) has a six-coordinate NaCl- or *anti*-NiAs-type structure.[18] Therefore, the small cations used in this study resulted in a different type of structure.

Table 1. Lattice constants, interionic distances, and radius ratio in the plastic phase

	Temperature[a]	Lattice constant	Interionic distance (Å)		Radius ratio[b]
	(K)	(Å)	Experimental	Calculated[c]	Calculated
[**1**][$CB_{11}H_{12}$]	430	7.70[e]	6.67	6.91	0.98
[**1**][$B(CN)_4$]	400	7.37[e]	6.38	6.46	0.89
[**2**][$B(CN)_4$][d]	353	7.50(5)	6.50	6.59	0.86
[**1**][OTf]	400	6.923(10)	5.99	6.15	0.80
[**2**][OTf]	400	7.08[e]	6.13	6.28	0.77
[**1**][CF_3BF_3]	293	6.841(3)	5.92	6.13	0.79
[**2**][CF_3BF_3]	293	7.025(4)	6.08	6.26	0.76
[**1**][BF_4]	430	6.60[e]	5.71	5.78	0.69
[**2**][BF_4]	293	6.76	5.86	5.91	0.66

[a]Temperature of the measurement. [b]Value of r^-/r^+ (or r^+/r^- for [**1**][$CB_{11}H_{12}$]), where the ionic radii are calculated from molecular volumes determined by density functional theory calculations. [c]Sum of the calculated radii of the cation and anion. [d]Ref. 20. [e]Calculated from the 110 peak owing to weak diffraction.

Phase transition temperatures and radius ratio. Based on the results of these and related salts,[17-20] we examine here the trend in the phase transition temperatures of ionic plastic crystals of sandwich complexes. A plot of the phase transition temperatures against the anion radius for various sandwich complex salts is shown in Figure 3a. It can be seen from this plot that the CF_3BF_3 salts tend to exhibit low transition temperatures. In addition, the salts with the bent anion $N(SO_2F)_2^-$ (FSA) exhibit higher transition temperatures than salts with other anions of similar size. Therefore, FSA is not an effective anion for cationic sandwich complexes, even though onium salts still give low transition temperatures with FSA.[35,36] In Figure 3b, the transition temperatures are plotted against the radius ratio. The dashed line in the figure represents the critical radius ratio (ρ = 0.73), which is the boundary between the six-coordinate and eight-coordinate structures according to the radius ratio rule.[34] Most of the salts investigated in this study having coordination number eight are located on the right of the dashed line, and their transition temperature tends to decrease with decreasing radius ratio. A plausible explanation for the tendency in terms of electrostatic interactions is that when approaching the critical radius ratio, the cations get closer to each other,

causing larger interionic repulsions, which facilitate molecular motion. However, the opposite trend is observed in octamethyl- and decamethylferrocenium salts. They have coordination number six with radius ratio below 0.73 (on the left-side of the dashed line in the figure), and their transition temperature tends to increase with decreasing radius ratio.[17,18] The contribution of Coulomb interactions should be small in these salts owing to many methyl groups, and steric effects should be dominant. With decreasing radius ratio, the contacts between the cations get larger, suppressing the molecular rotation due to steric hindrance of the methyl groups, which might explain the increase in the transition temperature.

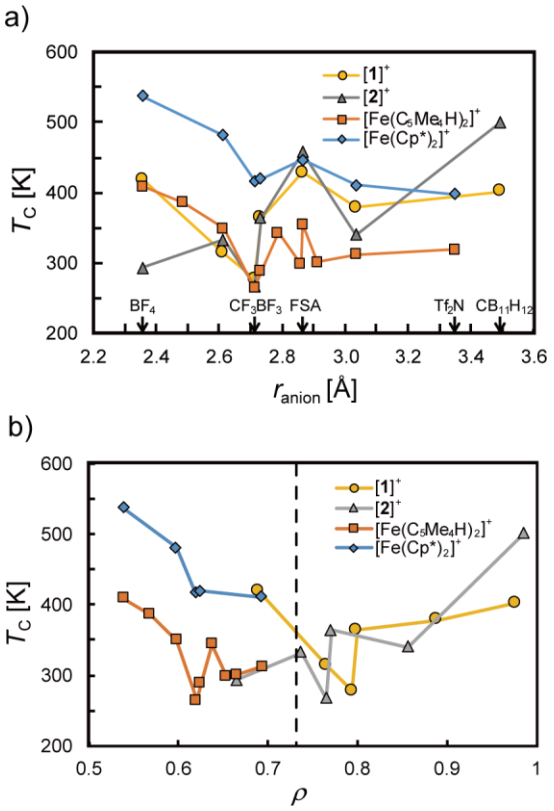

Figure 3. Phase transition temperatures of sandwich complex salts to the plastic phase plotted versus (a) the anion radius and (b) the radius ratio. The dashed line in b shows the critical radius ratio (ρ = 0.73). Panel b does not include data for FSA and Tf_2N salts because the anions are not spherical.

Low-temperature structures of salts with a plastic phase. The crystal structures of the

low-temperature phase (phase I) of [**1**][$CB_{11}H_{12}$], [**2**][$CB_{11}H_{12}$], [**1**][$B(CN)_4$], and [**2**][OTf] were determined. ORTEP drawings of the cations and anions are shown in Figure S3 (Supporting Information). The crystal structures of [**1**][OTf][32] and [**2**][$B(CN)_4$][20] are known. [**1**][$CB_{11}H_{12}$] and [**2**][$CB_{11}H_{12}$] are isomorphous among them. The anions and cations are alternately arranged in these salts, with one cation surrounded by eight anions. Therefore, the coordination numbers[37,38] of these salts in the low-temperature phase and in the plastic phase were identical, as also observed in octamethyl- and decamethylferrocenium salts.[17,18] The crystal structures of the CF_3BF_3 salts and [**2**][BF_4] could not be determined because they are plastic crystals at room temperature.

The packing diagram of [**2**][$CB_{11}H_{12}$] is shown in Figure 4a (space group $P2_1/n$, Z = 4). The structure of the isomorphous salt [**1**][$CB_{11}H_{12}$] is shown in Figure S4a (Supporting Information). The asymmetric unit of these salts contained a pair of cation and anion. The orientation of the anion was ordered. The B–C bonds (1.69–1.72 Å) are shorter than the B–B bonds (1.76–1.79 Å), which are comparable to literature values.[39,40] The transition temperature of [**2**][$CB_{11}H_{12}$] (T_C = 501 K) to the plastic phase was much higher than that of [**1**][$CB_{11}H_{12}$] (T_C = 402 K), as mentioned in the previous section, but their packing coefficients 100 K were comparable, at 67.8% and 67.4%, respectively. The asymmetric cation in [**2**][$CB_{11}H_{12}$] appears to be locked between the anions, hindering its isotropic rotation, which probably resulted in the high transition temperature of this salt.

To investigate the origin of the transition from phase I to phase II in these salts, we also determined the crystal structure of [**2**][$CB_{11}H_{12}$] in phase II (Figure 4b), although the analysis is incomplete owing to extensive disorder. In this phase, the space group was *C*mm2 (orthorhombic), exhibiting a higher symmetry than phase I ($P2_1/n$), and the lattice volume (Z = 2) was halved compared with phase I (Z = 4). The cation rings and anion exhibited extensive rotational disorder, whereas the long molecular axis of the cation was oriented along the *b*-axis. The phase transition in [**1**][$CB_{11}H_{12}$] may have the same feature. The larger phase transition entropy in [**2**][$CB_{11}H_{12}$] (14.7 J mol^{-1} K^{-1}) compared to [**1**][$CB_{11}H_{12}$] (6.6 J mol^{-1} K^{-1}) is likely due to the ring disorder in the

cation.

The packing diagram of [**1**][B(CN)$_4$] is shown in Figure 5 (space group $P2_1/c$, Z = 24). The asymmetric unit contained six cations and six anions. A short contact was observed between the N atom of the anion and the C atom of the cation, which was 0.1 Å shorter than the van der Waals distance (N···C = 3.14 Å). The alternate cation–anion arrangement in this salt is similar to that in [**2**][B(CN)$_4$] (space group $Cmc2_1$). However, [**2**][B(CN)$_4$] has a smaller unit cell (Z = 4), exhibiting a simpler molecular arrangement.[20]

The packing diagram of [**2**][OTf] (space group $P3_1$, Z = 9) is shown in Figure S4b (Supporting Information), but we refrain from a detailed discussion of this structure because the refinement was not complete owing to the disorder of anion. The asymmetric unit contained three anions and cations, and the molecular arrangement was somewhat similar to that in [**1**][OTf] ($P2_1/c$, Z = 12).[32] Unlike [**1**][OTf], there were no π–π contacts between the cations in this salt.

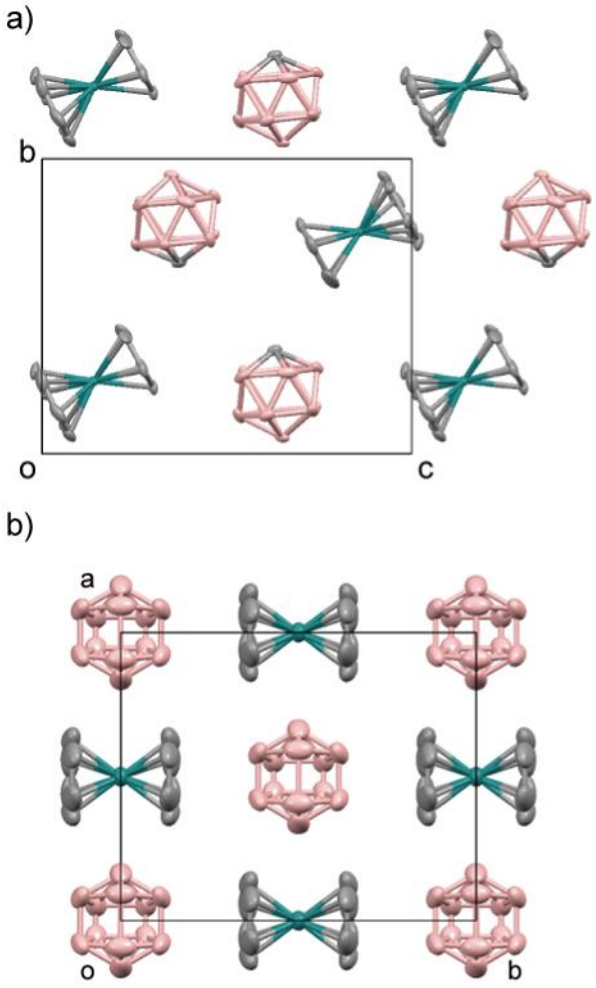

Figure 4. Packing diagram of [**2**][$CB_{11}H_{12}$] in (a) phase I and (b) phase II. Hydrogen atoms have been omitted. The structure of phase II contains extensive disorder (see text) and only part of the disordered moieties of each molecule is shown.

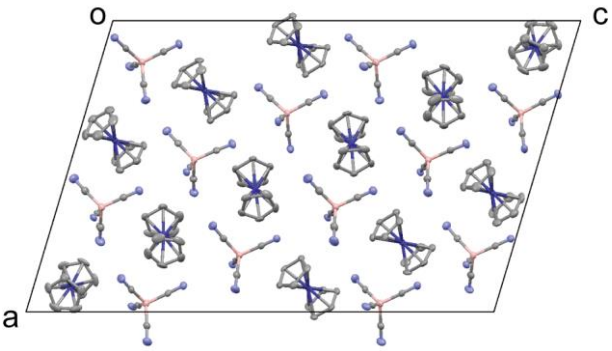

Figure 5. Packing diagram of [**1**][$B(CN)_4$]. Hydrogen atoms have been omitted.

Low-temperature structures of salts without plastic phases. In this section, we discuss the crystal structures of the $C(CN)_3$ and FAP salts at low temperature (phase I). These salts do not exhibit plastic phases. ORTEP drawings of the cations and anions in these salts are shown in Figure S3 (Supporting Information). The crystal structure of [**2**][$C(CN)_3$] has been reported previously.[20]

[**1**][$C(CN)_3$] and [**2**][$C(CN)_3$] are not isomorphic. They are exceptional in that they have no alternate arrangement of the cations and anions. Figure 6a shows the packing diagram of [**1**][$C(CN)_3$] (space group *C*2/*c*, *Z* = 4). The asymmetric unit contains half of the anion and half of the cation. The cation forms a columnar stacking structure, and there are π–π contacts between the cations, which are 0.15 Å shorter than the van der Waals distance (C···C distance: 3.25 Å). The cations are located between the anions and arranged linearly. The anion and the Cp ring of the cation are tilted by 57°, with no other π–π contacts between the anions. Six anions surround one cation, with five CN groups located around the Co atom (Co···NC distances: 4.29–4.67 Å). In [**2**][$C(CN)_3$], the anions also have a stacking structure through π–π contacts.[20] The structures and phase behaviors of these salts contrast those of [$Fe(C_5Me_4H)_2$][$C(CN)_3$], which has an alternate cation–anion arrangement and exhibits a plastic phase (T_C = 343.3 K).[18] The stacking structures of

the cations in [**1**][$C(CN)_3$] and [**2**][$C(CN)_3$], which have small and anisotropic Coulombic interactions, are probably responsible for the absence of a plastic phase and melting in these salts (T_m = 405.2 and 363.4 K, respectively). This result supports the conclusion that $C(CN)_3$ tends to form salts with low melting points,[20] which demonstrates the importance of crystal structure to the occurrence of the plastic phase.

[**1**][FAP] and [**2**][FAP] are isomorphous (space group $P2_1/n$, Z = 4), and their packing diagrams are shown in Figure 6b and Figure S4c (Supporting Information), respectively. with one crystallographically independent cation and anion. The cations and anions are arranged nearly alternately in the crystal. The cations are disordered in both salts. One of the Cp rings in [**1**][FAP] has a two-fold rotational disorder with a 0.5:0.5 occupancy, whereas the Cp and benzene rings in [**2**][FAP] are disordered with an occupancy of 0.5:0.5. The crystal structures of several FAP salts have been reported, which display similar conformation of the anion.[41-44]

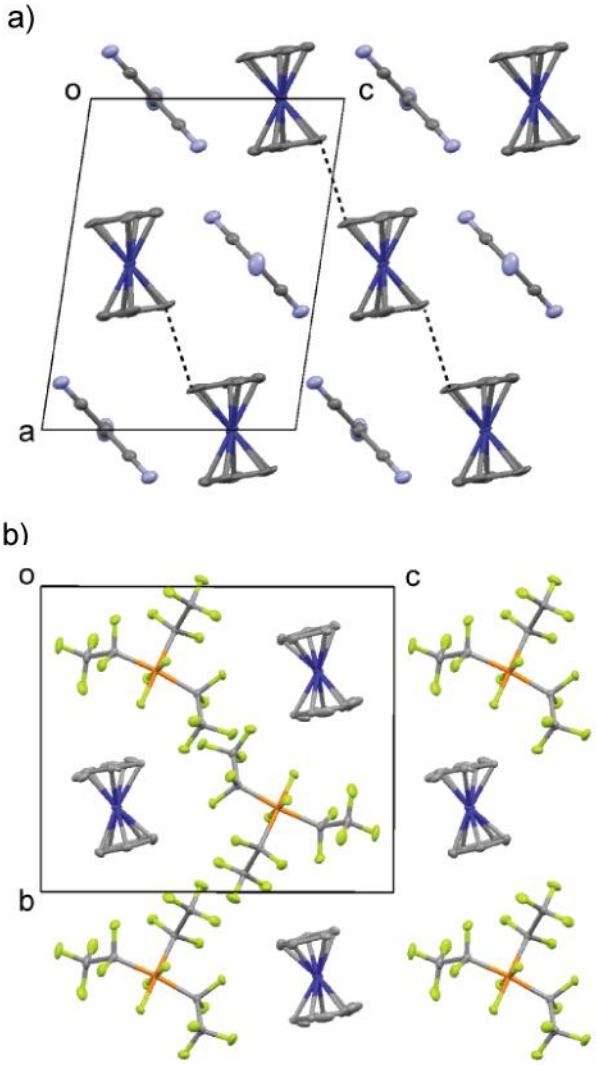

Figure 6. (a) Packing diagrams of [**1**][$C(CN)_3$] and (b) [**1**][FAP]. Hydrogen atoms have been omitted. The dotted lines in panel a represent the π–π contact.

CONCLUSION

Based on the present results and previous studies, a comprehensive understanding of the phase transition to the plastic phase of sandwich complex salts has been obtained. In this study, we investigated the thermal properties and crystal structures of salts of $[CoCp_2]^+$ and $[Ru(Cp)(C_6H_6)]^+$ with various anions. These salts have coordination number eight in the plastic phase, and the phase transition temperature generally increases with increasing anion volume. This contrasts the tendency found in octamethyl- and decamethylferrocenium salts, which have coordination number six. Furthermore, the coordination numbers in the low-temperature phase and the plastic phase are

identical, indicating that the structure of the plastic phase can be predicted from the low-temperature structure.

We found that CF_3BF_3 is a useful anion for lowering the phase transition temperature of sandwich complex salts. The CF_3BF_3 salts exhibited plastic phases below room temperature, exhibiting the lowest transition temperatures among the sandwich complex salts ever reported. In contrast, the $CB_{11}H_{12}$ salts exhibited very high phase transition temperatures despite their spherical anions, which is probably due to the large volume of the anion. The results also support the importance of molecular arrangement and anion shape to the occurrence of a plastic phase. The $C(CN)_3$ salts, which have no alternate cation–anion arrangement, and FAP salts, which have non-spherical anions, did not exhibit plastic phases.

These systematic investigations revealed the factors affecting the transition temperatures to the plastic phase in sandwich complex salts. These results may also be useful for the design of ionic plastic crystals with other cations. Based on these findings, we are currently investigating the electronic properties of organometallic ionic plastic crystals.

EXPERIMENTAL SECTION

General. $[CoCp_2]Cl$[45] and $[Ru(Cp)(C_6H_6)]Cl$[20] were prepared according to methods reported in the literature. $[CoCp_2][BF_4]$[33] and $[Ru(Cp)(C_6H_6)][BF_4]$[46] were produced by anion exchange using the corresponding chloride salts. $[CoCp_2][OTf]$[32] was prepared by the reaction of $[CoCp_2]Cl$ and AgOTf. Na[FAP] was prepared by cation exchange from [Bmim][FAP]. Other chemicals were purchased from commercial sources. DSC measurements were performed using a TA Instruments Q100 differential scanning calorimeter at a rate of 10 K min^{-1}. The phase transition to the plastic phase was also confirmed by observation of the loss of birefringence using a polarization microscope. Infrared spectra were recorded via attenuated total reflectance (ATR diamond)using a Thermo Scientific Nicolet iS 5 FT-IR spectrometer. Electrospray ionization–mass spectrometry spectra were recorded using a Thermo Fisher Scientific LTQ Orbitrap Discovery system. Powder

XRD measurements were performed using a Rigaku SmartLab diffractometer at room temperature and a Bruker APEX II Ultra at high temperatures. Indexing of the powder XRD data was performed using Rigaku PDXL software. The packing coefficients were calculated using PLATON.[47] The van der Waals volumes and ovalities of the cations and anions were estimated based on density functional theory calculations (B3LYP/LanL2DZ) using Spartan ′16 (Wavefunction, Inc.). The ionic radii were calculated assuming spheres of the same volumes as the ions. The ovality is the ratio of the calculated surface area to the minimum surface area of a molecule—the latter is the surface of a sphere with a volume that equals the actual volume of the molecule. The calculated values for the anions are listed in **Table S1** (Supporting Information).

Preparation of salts. *$[CoCp_2][CB_{11}H_{12}]$ ($[\mathbf{1}][CB_{11}H_{12}]$).* An aqueous solution (0.8 mL) of $Cs[CB_{11}H_{12}]$ (46 mg, 0.17 mmol) was added to an aqueous solution (0.1 mL) of $[CoCp_2]Cl$ (30 mg, 0.13 mmol). The mixture was stirred for 30 min and subsequently filtered, and the filtrate was evaporated under reduced pressure and dried under vacuum. The residue was dissolved in dichloromethane and filtered, and the filtrate was evaporated and dried under vacuum. Slow diffusion of diethyl ether into an acetone solution of the solid for three days at –6 °C precipitated yellow block crystals of the desired product, which were collected by filtration and dried under vacuum (16.0 mg, yield 37%). HRMS *m/z* calcd. for $[C_{10}H_{10}Co]^+$: 189.0115. Found: 189.0108. calcd. for $[CB_{11}H_{12}]^-$: 143.2035. Found: 143.2048. IR (cm^{-1}): 3107, 2525, 1414, 1088, 1063, 1019, 1008, 860, 715.

$[CoCp_2][B(CN)_4]$ ($[\mathbf{1}][B(CN)_4]$). An aqueous solution (0.5 mL) of $KB(CN)_4$ (54 mg, 0.35 mmol) was added to an aqueous solution (0.3 mL) of $[CoCp_2]Cl$ (35 mg, 0.15 mmol). The mixture was stirred for 30 min and then filtered, and the filtrate was evaporated under reduced pressure and dried under vacuum. The residue was extracted three times with dichloromethane (20 mL) and washed with water. The organic layer was dried over magnesium sulfate and filtered, and the solvent was evaporated under reduced pressure. The crude product was dissolved in dichloromethane–diethyl ether and the solution was cooled slowly to −40 °C. The product was

obtained as yellow block crystals (yield 13.7 mg, 26%). Anal. Calcd. for $C_{14}H_{10}N_4BCo$: C, 55.31; H, 3.32; N, 18.43. Found: C, 55.29; H, 3.34; N, 18.47. IR (cm^{-1}): 3117, 1416, 1009, 924, 861, 820.

*[CoCp$_2$][CF$_3$BF$_3$] ([**1**][CF$_3$BF$_3$]).* An aqueous solution (0.2 mL) of KCF_3BF_3 (54 mg, 0.31 mmol) was added to an aqueous solution (0.2 mL) of [CoCp$_2$]Cl (44 mg, 0.20 mmol). The mixture was stirred for 1 h and filtered, and the filtrate was evaporated under reduced pressure. The residue was washed with diethyl ether and dried under vacuum. Recrystallization of the solid from dichloromethane–hexane (−40 °C) gave the desired product as yellow needle crystals (12.4 mg, yield 24%). Anal. Calcd. for $C_{11}H_{10}F_6BCo$: C, 40.54; H, 3.09; N, 0.00. Found: C, 40.43; H, 2.88; N, 0.08. IR (cm^{-1}): 632, 724, 863, 948, 975, 1009, 1040, 1186, 1417, 3124.

*[CoCp$_2$][C(CN)$_3$] ([**1**][C(CN)$_3$]).* An aqueous solution (0.3 mL) of $KC(CN)_3$ (75 mg, 0.58 mmol) was added to an aqueous solution (0.2 mL) of [CoCp$_2$]Cl (59 mg, 0.26 mmol). The mixture was stirred for 30 min and filtered, and the filtrate was evaporated under reduced pressure and dried under vacuum. The residue was dissolved in water (2 mL) and extracted with dichloromethane. The organic layer was washed with water and dried over magnesium sulfate, and the solvent was evaporated under reduced pressure. Recrystallization of the solid from acetone–diethyl ether (−40 °C) gave the desired product as yellow needle crystals. The yield was not determined because the salt was very hygroscopic. HRMS *m/z* calcd. for $[C_{10}H_{10}Co]^+$: 189.0115. Found: 189.0103. Calcd. for $[C(CN)_3]^-$: 90.0092. Found: 90.0101.

*[CoCp$_2$][FAP] ([**1**][FAP]).* This salt was prepared as described for [**1**][CF_3BF_3] using Na[FAP] (41 mg, 0.09 mmol) and [CoCp$_2$]Cl (29 mg, 0.13 mmol). Recrystallization of the product from dichloromethane–diethyl ether (−40 °C) gave the desired product as yellow needle crystals (9.6 mg, yield 15%). Anal. Calcd. for $C_{16}H_{10}F_{18}PCo$: C, 30.31; H, 1.59; N, 0.00. Found: C, 30.11; H, 1.05; N, 0.25. IR (cm^{-1}): 1420, 1295, 1209, 1177, 1137, 1125, 1096, 1069, 1014, 974, 962, 865, 804, 764, 724, 617, 581, 530.

*[Ru(Cp)(C$_6$H$_6$)][CB$_{11}$H$_{12}$] ([**2**][CB$_{11}$H$_{12}$]).* This salt was prepared as described for [**1**][$CB_{11}H_{12}$] using [Ru(Cp)(C_6H_6)]Cl (12 mg, 0.04 mmol) and Cs[$CB_{11}H_{12}$] (14 mg, 0.05 mmol). The desired

product was obtained as colorless block crystals (8.2 mg, yield 49%). HRMS *m/z* calcd. for $[C_{11}H_{11}Ru]^+$: 244.9904. Found: 244.9899. calcd. for $[CB_{11}H_{12}]^-$: 143.2035. Found: 143.2047. IR (cm^{-1}): 2527, 1442, 1087, 1062, 1018, 982, 843, 821, 715, 543.

*[RuCp(C_6H_6)][OTf] ([**2**][OTf]).* An aqueous solution (0.3 mL) of AgOTf (71 mg, 0.28 mmol) was added to an aqueous solution (0.4 mL) of [RuCp(C_6H_6)]Cl (42 mg, 0.14 mmol), and the mixture was stirred for 30 min and collected by decantation. The residue was extracted twice with water, and the water solution was combined with the water phase. After evaporation of water, the residue was dried under vacuum. Recrystallization of the solid from acetone–diethyl ether (−40 °C) gave the desired product as colorless needle crystals (36.2 mg, yield 64%). Anal. Calcd. for $C_{12}H_{11}O_3F_3SRu$: C, 36.64; H, 2.82; N, 0.00. Found: C, 36.57; H, 2.47; N, 0.02. IR (cm^{-1}): 3085, 1442, 1417, 1256, 1221, 1147, 1028, 1012, 829, 754, 634, 571.

*[RuCp(C_6H_6)][CF_3BF_3] ([**2**][CF_3BF_3]).* This salt was prepared as described for [**1**][CF_3BF_3] using [Ru(Cp)(C_6H_6)]Cl (44 mg, 0.16 mmol) and KCF_3BF_3 (47 mg, 0.27 mmol). The product was obtained as colorless crystals (28.5 mg, yield 48%). Anal. Calcd. for $C_{12}H_{11}F_6BRu$: C, 37.82; H, 2.91; N, 0.00. Found: C, 37.83; H, 2.57; N, 0.06. IR (cm^{-1}): 632, 724, 826, 852, 948, 975, 1011, 1042, 1158, 1417, 1444, 3121.

*[RuCp(C_6H_6)][FAP] ([**2**][FAP]).* This salt was prepared as described for [**1**][FAP] using [Ru(Cp)(C_6H_6)]Cl (62 mg, 0.21 mmol) and Na[FAP] (290 mg, 0.65 mmol). Recrystallization of the crude product from dichloromethane (−40 °C) gave the desired product as pale yellow crystals (40.3 mg, yield 46%). Anal. Calcd. for $C_{16}H_{10}F_{18}PRu$: C, 29.62; H, 1.61; N, 0.00. Found: C, 29.74; H, 1.38; N, 0.08. IR (cm^{-1}): 1209, 1180, 1136, 1125, 721, 615.

X-ray crystallography. Single crystals of [**1**][$C(CN)_3$], [**1**][FAP], and [**2**][FAP] suitable for X-ray crystallography were obtained by recrystallization from acetone–diethyl ether, dichloromethane–diethyl ether, and dichloromethane, respectively. Single crystals of other salts were grown by diffusion of diethyl ether into acetone solutions. The crystal of [**1**][$C(CN)_3$] was collected after adding liquid paraffin to the mother liquor owing to deliquescence. Single-crystal

XRD data were collected using a Bruker APEX II Ultra CCD diffractometer with MoKα radiation (λ = 0.71073 Å). The structures were determined by the direct method using SHELXL.[48] The crystallographic parameters are shown in **Tables S2**–**S4** (Supporting Information). We also tried to determine the crystals structures of [**2**][$CB_{11}H_{12}$] and [**2**][OTf], but their refinements were unsatisfactory because of disorder.

ASSOCIATED CONTENT

Supporting Information

DSC traces (Figure S1), powder X-ray diffraction patterns (Figure S2), ORTEP drawing of the molecular structures (Figure S3), and packing diagrams (Figure S4). This information is available free of charge via the internet at http://pubs.acs.org/.

Accession Codes

CCDC-1839707 ([**1**][$CB_{11}H_{12}$]), -1850224 ([**2**][$CB_{11}H_{12}$]), -1843938 ([**1**][$B(CN)_4$]), -1825249 ([**1**][$C(CN)_3$]), -1825248 ([**1**][FAP]), and -1835966 ([**2**][FAP]) contain the supplementary crystallographic data for this paper. These data can be obtained free of charge from The Cambridge Crystallographic Data Centre via www.ccdc.cam.ac.uk/data_request/cif.

AUTHOR INFORMATION

Corresponding Author

*E-mail: tmochida@platinum.kobe-u.ac.jp. Tel/Fax: +81-78-803-5679.

ORCID

Tomoyuki Mochida: 0000-0002-3446-2145

Notes

The authors declare no competing financial interest.

ACKNOWLEDGMENTS

We thank Dr. Yusuke Funasako (Sanyo-Onoda City University) and Takumi Tominaga (Kobe University) for their help with X-ray crystallographic analysis. This work was financially supported by KAKENHI (grant number 16H04132) from the Japan Society for the Promotion of Science (JSPS).

REFERENCES

(1) MacFarlane, D. R; Huang, J.; Forsyth, M. Lithium-doped plastic crystal electrolytes exhibiting fast ion conduction for secondary batteries. *Nature* **1999**, *402*, 792–794.

(2) Pringle, J. M. Recent progress in the development and use of organic ionic plastic crystal electrolytes. *Phys. Chem. Chem. Phys*. **2013**, *15*, 1339–1351.

(3) Abu-Lebdeh, Y.; Alarco, P.-J.; Armand, M. Conductive Organic Plastic Crystals Based on Pyrazolium Imides. *Angew. Chem. Int. Ed.* **2003**, *42*, 4499–4501.

(4) Luo, J.; Jensen, A. H.; Brooks, N. R.; Sniekers, J.; Knipper, M.; Aili, D.; Li, Q.; Vanroy, B.; Wübbenhorst, M.; Yan, F.; Meervelt, L. V.; Shao, Z.; Fang, J.; Luo, Z.-H.; De Vos, D. E.; Binnemans, K.; Fransaer, J. 1,2,4-Triazolium perfluorobutanesulfonate as an archetypal pure protic organic ionic plastic crystal electrolyte for all-solid-state fuel cells. *Energy Environ. Sci.* **2015**, *8*, 1276–1291.

(5) Lee, M.; Choi, U. H.; Wi, S.; Slebodnick, C.; Colby, R. H.; Gibson, H. W. 1,2-Bis[*N*-(*N*′-alkylimidazolium)]ethane salts: a new class of organic ionic plastic crystals. *J. Mater. Chem.* **2011**, *21*, 12280–12287.

(6) de Pedro, I.; García-Saiz, A.; González, J. A.; Ruiz de Larramendi, I.; Rojo, T.; Afonso, C.; Simeonov, S.; Waerenborgh, J. C.; Blanco, J. A.; Ramajo, B.; Rodríguez, J. Magnetic ionic plastic crystal: choline[$FeCl_4$]. *Phys. Chem. Chem. Phys*. **2013**, *15*, 12724–12733.

(7) Henderson, W. A.; Herstedt, M.; Young, V. G.; Passerini, Jr., S.; De Long, H. C.; Trulove, P. C. New Disordering Mode for $TFSI^-$ Anions: The Nonequilibrium, Plastic Crystalline Structure of Et_4NTFSI. *Inorg. Chem.* **2006**, *45*, 1412–1414;

(8) Henderson, W. A.; Young, V. G., Jr.; Passerini, S.; Trulove, P. C.; De Long, H. C. Plastic Phase Transitions in *N*-Ethyl-*N*-methylpyrrolidinium Bis(trifluoromethanesulfonyl)imide. *Chem. Mat.* **2006**, *18*, 934–938.

(9) Lauw, Y.; Rüther, T.; Horne, M. D.; Wallwork, K. S.; Skelton, B. W.; Madsen, I. C.; Rodopoulos, T. Structural Studies on the Basic Ionic Liquid 1-Ethyl-1,4-diazabicyclo[2.2.2]octanium Bis(trifluoromethylsulfonyl)imide and Its Bromide Precursor. *Cryst. Growth Des.* **2012**, *12*, 2803–2813.

(10) Ishida, H.; Iwachido, T.; Hayama, N.; Ikeda, R.; Terashima, M.; Nakamura, D. Self-Diffusion and Reorientation of Methylammonium Ions in $(CH_3NH_3)_2ZnCl_4$ Crystals as Studied by ^{1}H-NMR. *Z. Naturforsch.* **1989**, *44A*, 741–746.

(11) Matsumoto, K.; Harinaga, U.; Tanaka, R.; Koyama, A.; Hagiwara, R.; Tsunashima, K. The structural classification of the highly disordered crystal phases of [N_n][BF_4], [N_n][PF_6], [P_n][BF_4], and [P_n][PF_6] salts (N_n^+= tetraalkylammonium and P_n^+ = tetraalkylphosphonium). *Phys. Chem. Chem. Phys*. **2014**, *16*, 23616–23626.

(12) Enomoto, T.; Kanematsu, S.; Tsunashima, K.; Matsumoto, K.; Hagiwara, R. Physicochemical properties and plastic crystal structures of phosphonium fluorohydrogenate salts. *Phys. Chem. Chem. Phys.* **2011**, *13*, 12536–12544.

(13) Zhou, Z.-B.; Matsumoto, H. Lithium-doped, organic ionic plastic crystal electrolytes exhibiting high ambient-temperature conductivities. *Electrochem. Commun.* **2007**, *9*, 1017–1022.

(14) Hayasaki, T.; Hirakawa, S.; Honda, H. New Ionic Plastic Crystals of NR_4BEt_3Me (R = Me and Et) and $NR_xR'_{4-x}BEt_3Me$ (R = Et, R′ = Me and Pr, x = 1–3) in a New Class of Plastic Crystals. *Bull. Chem. Soc. Jpn.* **2013**, *86*, 993–1001.

(15) Timmermans, J. Plastic Crystals: a Historical Review. *J. Phys. Chem. Solids* **1961**, *18*, 1–8.

(16) *The Plastically Crystalline State: Orientationally Disordered Crystals*, Sherwood, J.; John Wiley & Sons:

Chichester, UK, (1979).

(17) Mochida, T.; Funasako, Y.; Ishida, M.; Saruta, S.; Kosone, T.; Kitazawa, T. Crystal Structures and Phase Sequences of Metallocenium Salts with Fluorinated Anions: Effects of Molecular Size and Symmetry on Phase Transitions to Ionic Plastic Crystals. *Chem. Eur. J*. **2016**, *22*, 15725–15732.

(18) Mochida, T.; Ishida, M.; Tominaga, T.; Takahashi, K.; Sakurai, T.; Ohta, H. Paramagnetic ionic plastic crystals containing the octamethylferrocenium cation: counteranion dependence of phase transitions and crystal structures. *Phys. Chem. Chem. Phys.* **2018**, *20*, 3019–3028.

(19) Mochida, T.; Funasako, Y.; Inagaki, T.; Li, M.-J.; Asahara, K.; Kuwahara, D. Crystal Structures and Phase-Transition Dynamics of Cobaltocenium Salts with Bis(perfluoroalkylsulfonyl)amide Anions: Remarkable Odd–Even Effect of the Fluorocarbon Chains in the Anion. *Chem. Eur. J.* **2013**, *19*, 6257–6264.

(20) Tominaga, T.; Ueda, T.; Mochida, T. Effect of substituents and anions on the phase behavior of Ru(II) sandwich complexes: exploring the boundaries between ionic liquids and ionic plastic crystals. *Phys. Chem. Chem. Phys.* **2017**, *19*, 4352–4359.

(21) Inagaki, T.; Takahashi, M.; Kanadani, C.; Saito, T.; Mochida, T. Ionic Liquids of Cationic Sandwich Complexes. *Chem. Eur. J.* **2012**, *18*, 6795–6804.

(22) Funasako, Y.; Inagaki, T.; Mochida, T.; Sakurai, T.; Ohta, H.; Furukawa, K.; Nakamura, T. Organometallic ionic liquids from alkyloctamethylferrocenium cations: thermal properties, crystal structures, and magnetic properties. *Dalton Trans.* **2013**, *42*, 8317–8327.

(23) Komurasaki, A.; Funasako, Y.; Mochida, T. Colorless organometallic ionic liquids from cationic ruthenium sandwich complexes: thermal properties, liquid properties, and crystal structures of $[Ru(\eta^5\text{-}C_5H_5)(\eta^6\text{-}C_6H_5R)][X]$ ($X = N(SO_2CF_3)_2$, $N(SO_2F)_2$, PF_6). *Dalton. Trans.* **2015**, *44*, 7595–7605.

(24) Higashi, T.; Ueda, T.; Mochida, T. Effects of substituent branching and chirality on the physical properties of ionic liquids based on cationic ruthenium sandwich complexes. *Phys. Chem. Chem. Phys.* **2016**, *18*, 10041–10048.

(25) Webb, R. J.; Lowery, M. D.; Shiomi, Y.; Sorai, M.; Wittebort, R. J.; Hendrickson, D. N. Ferrocenium Hexafluorophosphate: Molecular Dynamics in the Solid State. *Inorg. Chem.* **1992**, *31*, 5211–5219.

(26) Grepioni, F.; Cojazzi, G.; Draper, S. M.; Scully, N.; Braga, D. Crystal Forms of Hexafluorophosphate Organometallic Salts and the Importance of Charge-Assisted C-H---F Hydrogen Bonds. *Organometallics* **1998**, *17*, 296–307.

(27) Grepioni, F.; Cojazzi, G.; Braga, D.; Marseglia, E.; Scaccianoce, L.; Johnson, B. F. G. Crystal architecture of the cocrystalline salt $[Ru(\eta^5\text{-}C_5H_5)(\eta^6\text{-trans-PhCH:CHPh})][PF_6]\cdot 0.5$ trans-PhCH=CHPh and the reversible order–disorder phase transition in $[Ru(\eta^5\text{-}C_5H_5)(\eta^6\text{-}C_6H_6)][PF_6]$ *J. Chem. Soc., Dalton Trans.* **1999**, 553–558.

(28) Schottenberger, H.; Wurst, K.; Griesser, U. J.; Jetti, R. K. R.; Laus, G.; Herber, R. H.; Nowik, I. ^{57}Fe-Labeled Octamethylferrocenium Tetrafluoroborate. X-ray Crystal Structures of Conformational Isomers, Hyperfine Interactions, and Spin−Lattice Relaxation by Moessbauer Spectroscopy. *J. Am. Chem. Soc*. **2005**, *127*, 6795–6801.

(29) Bukovsky, E. V.; Lacroix, M. R.; DeWeerd, N. J.; Reeves, B. J.; Kobayashi, Y.; Bayless, M. B.; Bradshaw, G. P.; Choi, Y. L.; Newell, B. S.; Strauss, S. H. Structures of 1,1′,3,3′-tetra(2-methyl-2-nonyl)ferrocenium(1+) salts of $CB_{11}H_{12}^-$, $B_{12}F_{12}^{2-}$, BF_4^-, PF_6^-, and ClO_3^-. *J. Organomet. Chem.* **2018**, *865*, 128–137.

(30) Zhou, Z.-B.; Matsumoto, H.; Tatsumi, K. Low-melting, Low-viscous, Hydrophobic Ionic Liquids: *N*-Alkyl(alkyl ether)-*N*-methylpyrrolidinium Perfluoroethyltrifluoroborate. *Chem Lett.* **2004**, *33*, 1636–1637.

(31) Zhou, Z.-B.; Matsumoto, H.; Tatsumi, K. Low-Melting, Low-Viscous, Hydrophobic Ionic Liquids: 1-

Alkyl(Alkyl Ether)-3-methylimidazolium Perfluoroalkyltrifluoroborate. *Chem. Eur. J.* **2004**, *10*, 6581–6591.

(32) Andrews, C. G.; Macdonald, C. L. B. Cobaltocenium trifluoromethanesulfonate. *Acta Cryst.* **2005**, *E61*, m2103–m2105.

(33) Cotton, F. A.; Daniels, L. M.; Wilkinson, C. C. A highly disordered cobaltocenium salt. *Acta. Cryst.* **2001**, *E57*, m529–m530.

(34) *Shriver and Atkins' Inorganic Chemistry*; 4th ed; Atkins, P.; Overton, T.; Rourke, J.; Weller, M.; Armstrong, F.; Oxford University Press, Oxford, 2010.

(35) Yunis, R.; Newbegin, T. W.; Hollenkamp, A. F.; Pringle, J. M. Ionic liquids and plastic crystals with a symmetrical pyrrolidinium cation. *Mater. Chem. Front.* **2018**, *2*, 1207–1214.

(36) Yoshizawa-Fujita, M.; Kishi, E.; Suematsu, M.; Takekawa, T.; Rikukawa, M. A Plastic Electrolyte Material in a Highly Desirable Temperature Range: *N*-Ethyl-*N*-methylpyrrolidinium Bis(fluorosulfonyl)amide. *Chem. Lett.* **2014**, *43*, 1909–1911.

(37) Mingos, D. M. P.; Rohl, A. L. Size and shape characteristics of inorganic molecules and ions and their relevance to molecular packing problems. *J. Chem. Soc., Dalton Trans*., **1991**, 3419–3425.

(38) Rohl, A. L.; Mingos, D. M. P. Size and shape of molecular ions and their relevance to the packing of the 'soft salts'. *Inorg. Chim. Acta*, **1993**, *212*, 5–13.

(39) McLemore, D. K.; Dixon, D. A.; Strauss, S. H. Density functional theory and fluorocarboranes: I. Trends in B–H and B–F distances and dissociation energies for $CB_{11}H_{12-n}F_n^-$ anions (n = 0, 1, 6, 11). *Inorg. Chim. Acta*, **1999**, *294*, 193–199.

(40) Douvris, C.; Michl, J. Update 1 of: Chemistry of the Carba-*closo*-dodecaborate(−) Anion, $CB_{11}H_{12}^-$. *Chem. Rev.* **2013**, *113*, PR179–PR233.

(41) Pliquett, D.; Schulz, P. S.; Heinemann, F. W.; Bause, A.; Wasserscheid, P. Liquid silver tris(perfluoroethyl)trifluorophosphate salts as new media for propene/propane separation. *Phys. Chem. Chem. Phys.* **2016**, *18*, 28242–28253.

(42) Solyntjes, S.; Neumann, B.; Stammler, H.-G.; Ignat'ev, N.; Hoge, B. Difluorotriorganylphosphoranes for the Synthesis of Fluorophosphonium and Bismuthonium Salts. *Eur. J. Inorg, Chem.* **2016**, *2016*, 3999–4010.

(43) Beichel, W.; Preiss, U. P.; Benkmil, B.; Steinfeld, G.; Eiden, P.; Kraft, A.; Krossing, I. Temperature Dependent Crystal Structure Analyses and Ion Volume Determinations of Organic Salts. *Z. Anorg. Allg. Chem.* **2013**, *639*, 2153–2161.

(44) Laus, G.; Schwärzler, A.; Schuster, P.; Bentivoglio, G.; Hummel, M.; Wurst, K.; Kahlenberg, V.; Lörting, T.; Schütz, J.; Peringer, P.; Bonn, G.; Nauer, G.; Schottenberger, H. *N,N'*-Di(alkyloxy)imidazolium Salts: New Patent-free Ionic Liquids and NHC Precatalysts. *Z. Naturforsch.* **2007**, *62b*, 295–308.

(45) Choi, K.; Gardner, D.; Hilbrandt, N.; Bein, T. Combinatorial Methods for the Synthesis of Aluminophosphate Molecular Sieves. *Angew. Chem. Int. Ed*. **1999**, *38*, 2891–2894.

(46) Vol'kenau, N. A.; Bolesova, I. N.; Shul'pina, L. S.; Kitaigorodskii, A. N. Reactivity of arenecyclopentadienylruthenium cations. *J. Organomet. Chem.* **1984**, *267*, 313–321.

(47) Spek, A. L. Structure validation in chemical crystallography. *Acta Cryst*allogr. **2009**, *D65*, 148–155.

(48) Sheldrick, G. M. A short history of SHELX. *Acta Crystallogr.* **2008**, *A64*, 112–122.

For Table of Contents Use Only

Title: Effects of Molecular Structure on Phase Transitions of Ionic Plastic Crystals Containing Cationic Sandwich Complexes

Authors: H. Kimata and T. Mochida*

SYNOPSIS. We investigated phase transition to the ionic plastic phase in salts of sandwich complexes with various anions and revealed the correlation between phase transition temperatures, crystal structures, and molecular structures. The phase transition temperature tended to decrease with decreasing radius ratio. Several salts exhibited a plastic phase below room temperature.

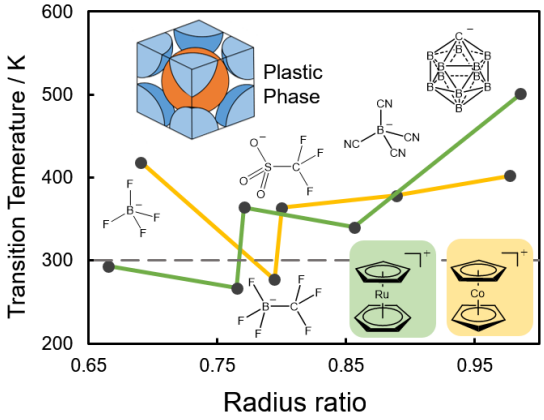

Supporting Information

Effects of Molecular Structure on Phase Transitions of Ionic Plastic Crystals Containing Cationic Sandwich Complexes

Hironori Kimata and Tomoyuki Mochida*

Department of Chemistry, Graduate School of Science, Kobe University, Rokkodai, Nada, Hyogo 657-8501, Japan. E-mail: tmochida@platinum.kobe-u.ac.jp

(a) [**1**][$CB_{11}H_{12}$]

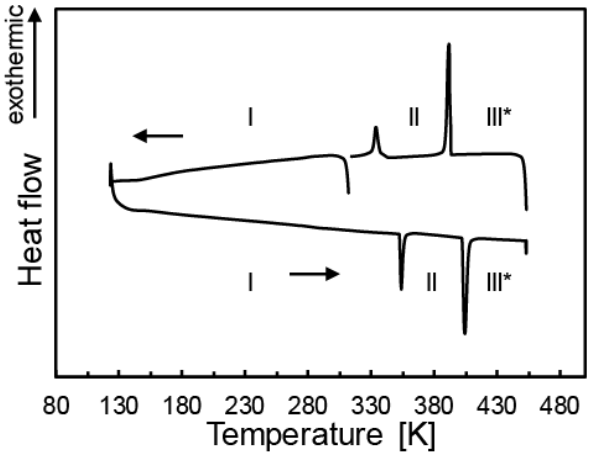

(b) [**1**][$B(CN)_4$]

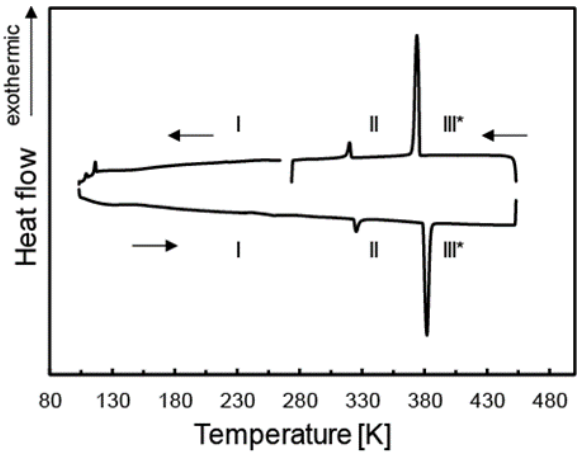

(c) [**1**][OTf]

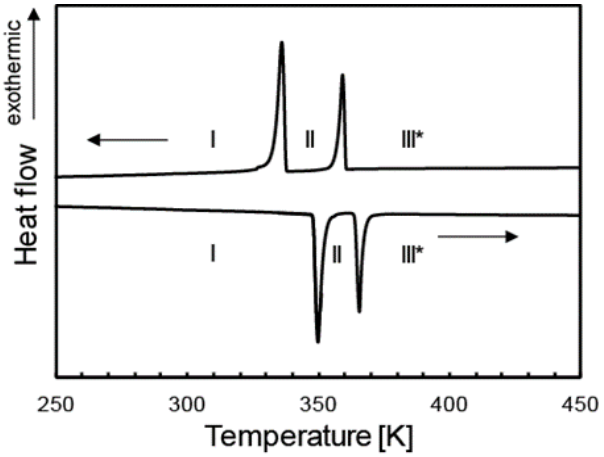

(d) [**1**][CF_3BF_3]

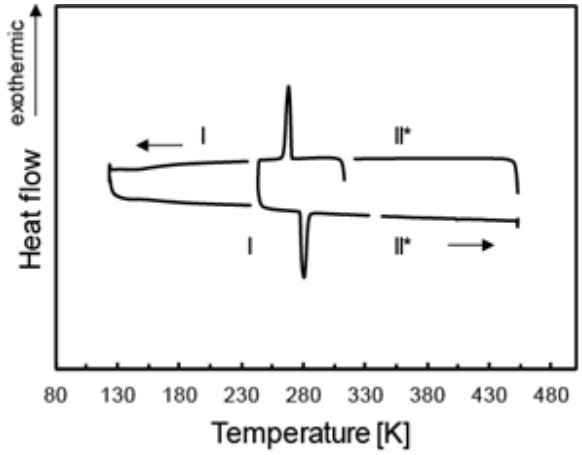

(e) [**1**][BF_4]

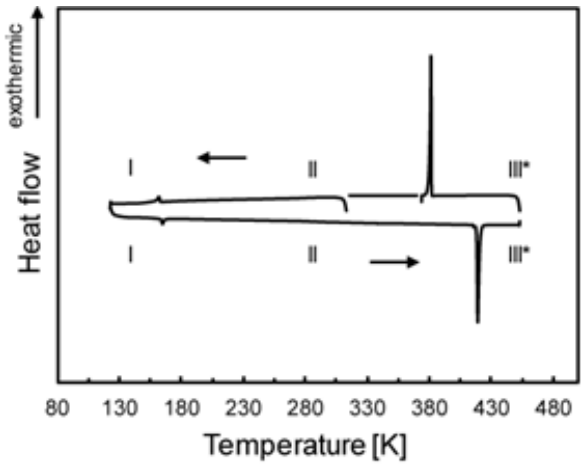

(f) [**1**][$C(CN)_3$]

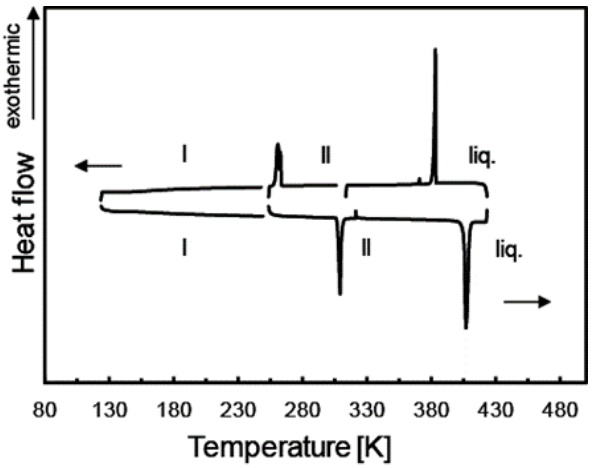

(g) [**1**][FAP]

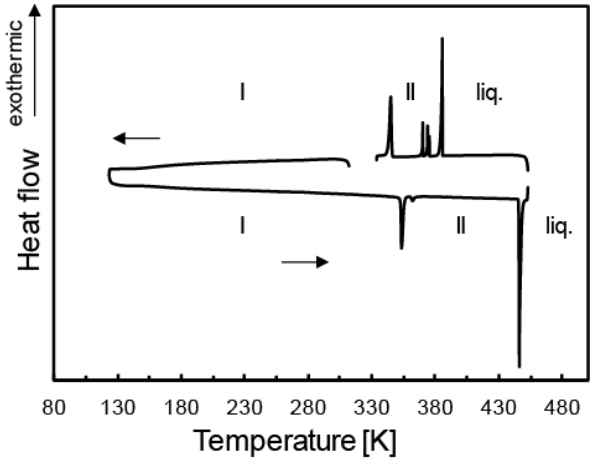

(h) [**2**][$CB_{11}H_{12}$]

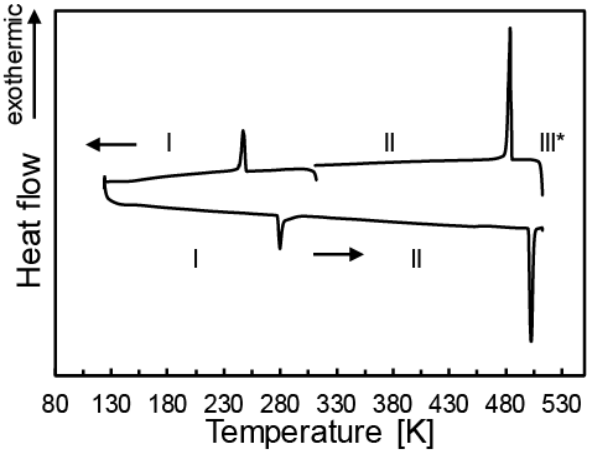

(i) [**2**][OTf]

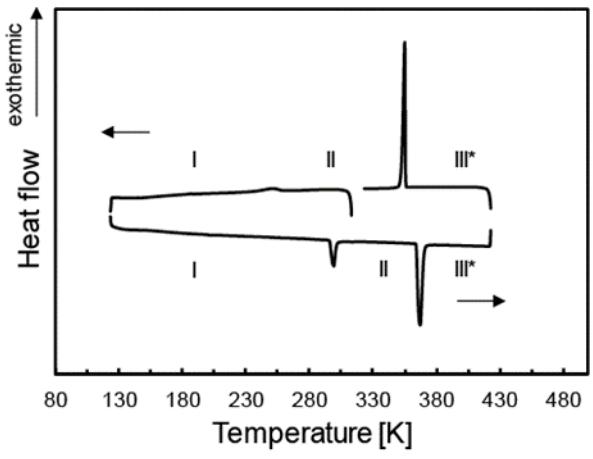

(j) [**2**][CF_3BF_3]

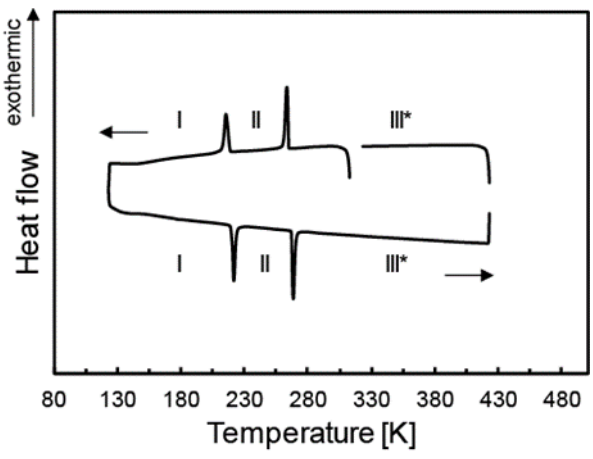

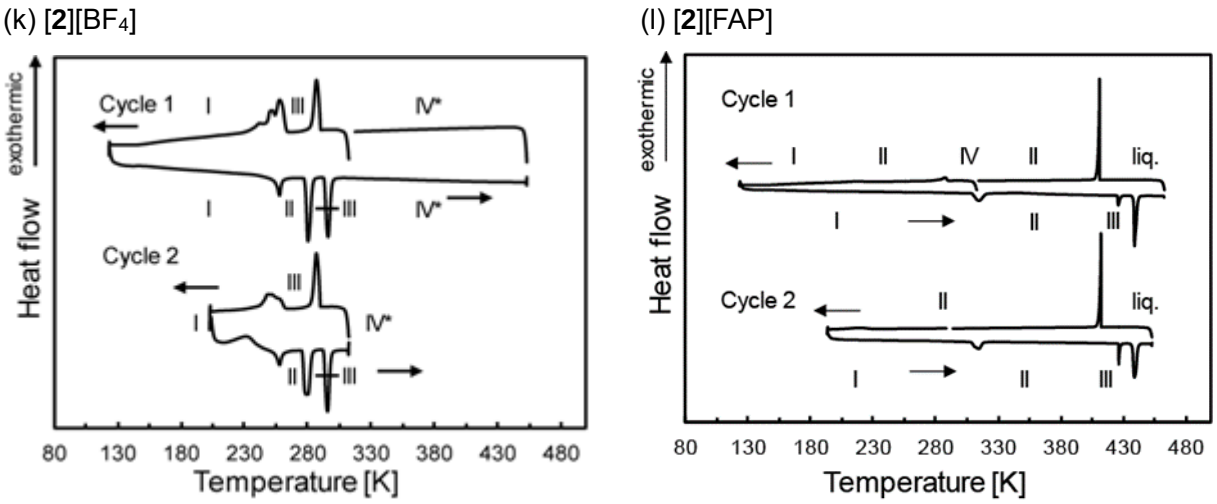

Figure S1. DSC traces of (a) [**1**][$CB_{11}H_{12}$], (b) [**1**][$B(CN)_4$], (c) [**1**][OTf], (d) [**1**][CF_3BF_3], (e)[**1**][BF_4] (f)[**1**][$C(CN)_3$], (g) [**1**][FAP], (h) [**2**][$CB_{11}H_{12}$], (i) [**2**][OTf], (j) [**2**][CF_3BF_3], (k) [**2**][BF_4], and (l) [**2**][FAP].

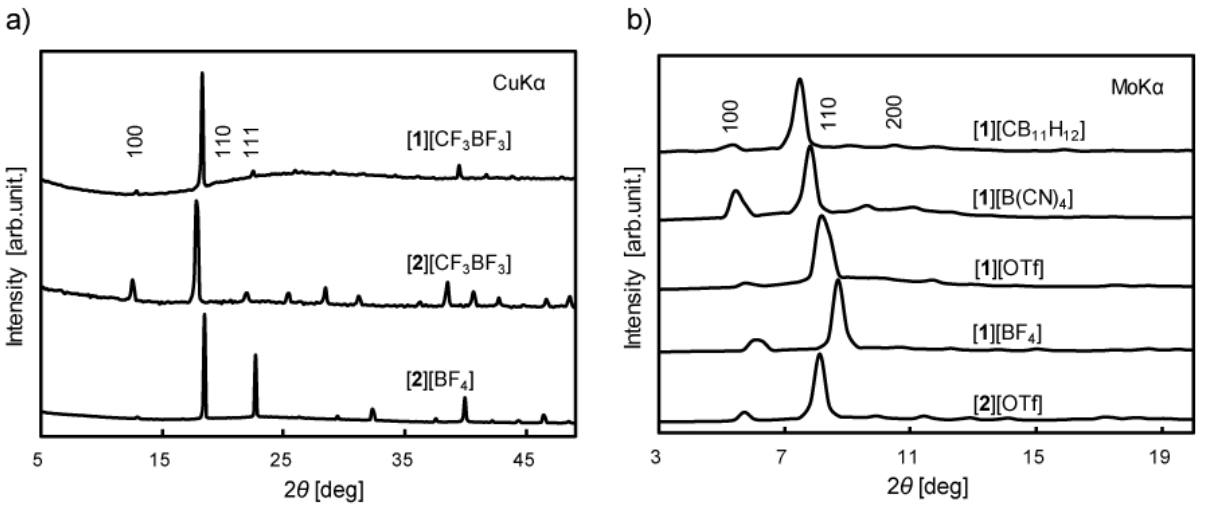

Figure S2. Powder X-ray diffraction patterns of plastic phases. (a) [**1**][CF_3BF_3], [**2**][CF_3BF_3] and [**2**][BF_4] at 293 K (CuKα radiation), (b) [**1**][OTf], [**2**][OTf], and [**1**][$B(CN)_4$] at 400 K, [**1**][$CB_{11}H_{12}$] and [**1**][BF_4] at 430 K (MoKα radiation).

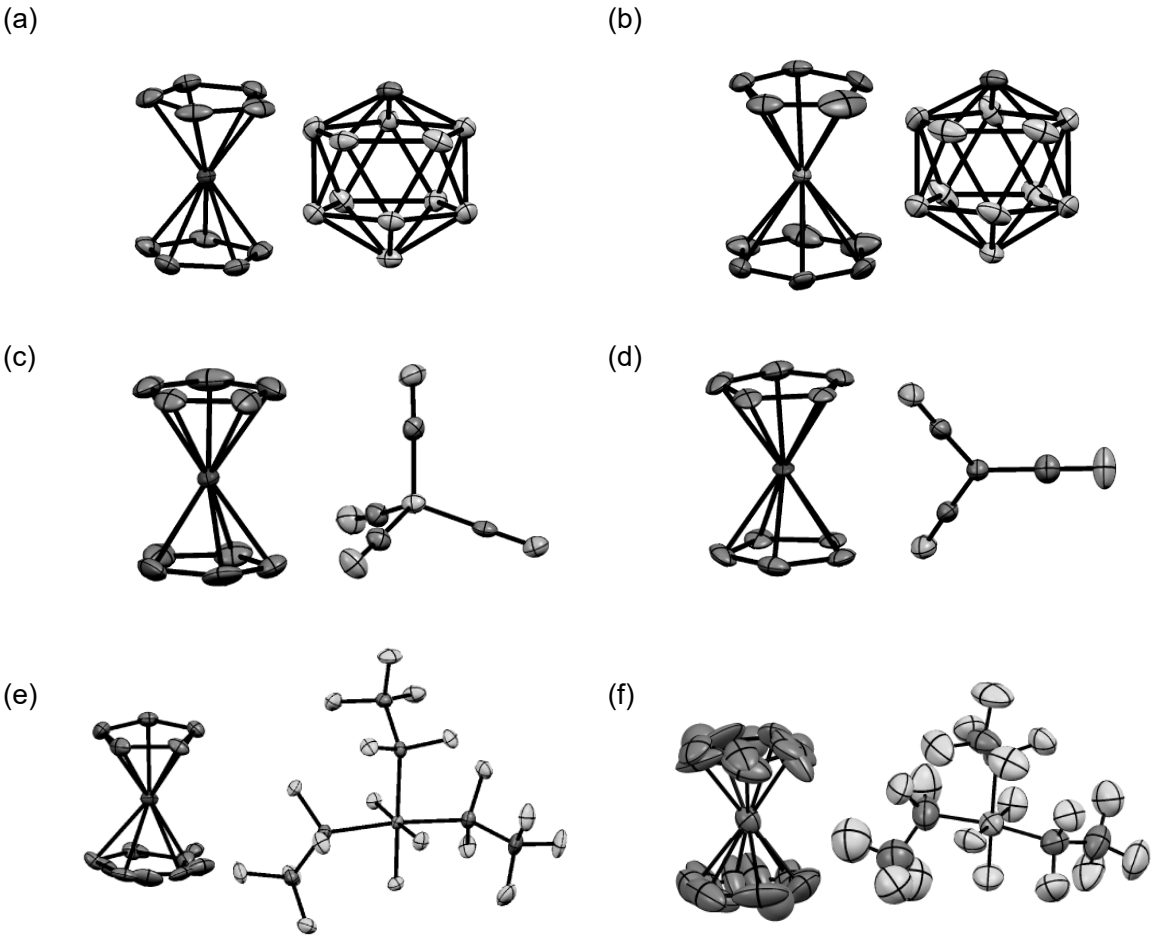

Figure S3. ORTEP drawings of the cations and anions in (a) [**1**][$CB_{11}H_{12}$], (b) [**2**][$CB_{11}H_{12}$], (c) [**1**][$B(CN)_4$], (d) [**1**][$C(CN)_3$], (e) [**1**][FAP], and (f) [**2**][FAP]. Hydrogen atoms have been omitted for clarity.

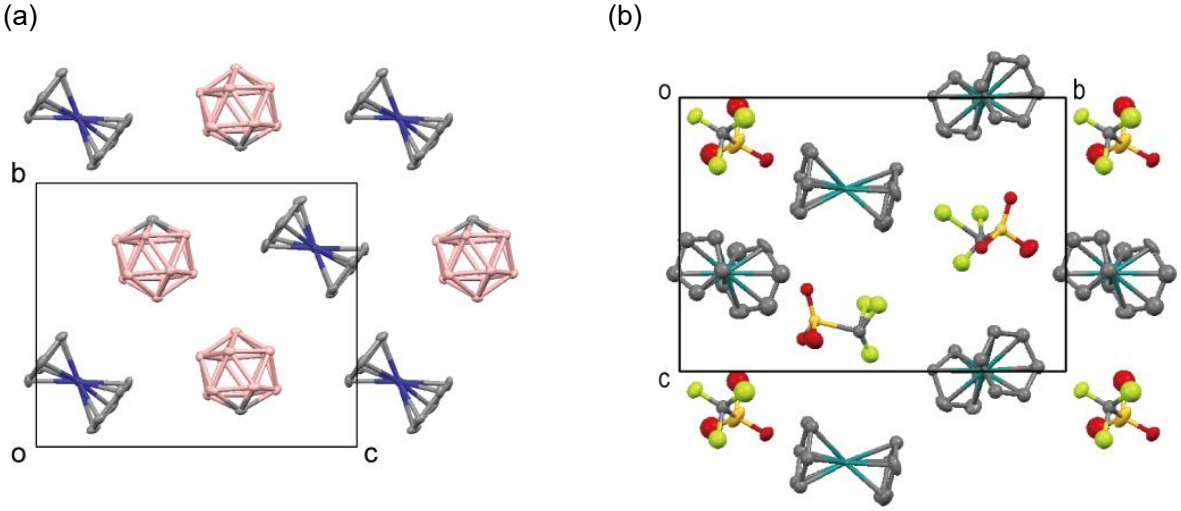

(c)

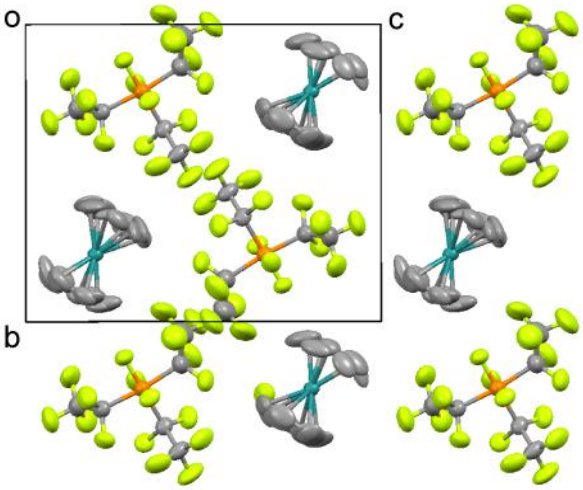

Figure S4. Packing diagrams of (a) [**1**][$CB_{11}H_{12}$], (b) [**2**][OTf] (only one of the disordered moieties in the anion is shown), and (c) [**2**][FAP]. Hydrogen atoms have been omitted for clarity.

Table S1. van der Waals volumes and ovalities of anions estimated based on DFT calculations (B3LYP/LanL2DZ)

molecule	volume (Å^3)	ovality
BF_4^-	54.9	1.10
$N(CN)_2^-$	64.5	1.12
PF_6^-	74.9	1.20
$CF_3BF_3^-$	83.6	1.19
OTf^-	85.4	1.23
$C(CN)_3^-$	90.8	1.17
$FeCl_4^-$	98.0	1.45
FSA	98.7	1.33
$GaCl_4^-$	103.4	1.29
$B(CN)_4^-$	117.2	1.22
Tf_2N^-	157.5	1.44
Monocarba-*closo*-dodecaborate	178.7	1.12
FAP	243.2	1.40

Table S2. Crystallographic parameters

	[**1**][$CB_{11}H_{12}$]	[**2**][$CB_{11}H_{12}$]	[**1**][$B(CN)_4$]	[**1**][$C(CN)_3$]
Empirical formula	$C_{11}H_{22}B_{11}Co$	$C_{12}H_{23}B_{11}Ru$	$C_{14}H_{10}BN_4Co$	$C_{14}H_{10}N_3Co$
Formula weight	332.12	387.28	304.00	279.18
Crystal system	Monoclinic	Monoclinic	Monoclinic	Monoclinic
Space group	$P2_1/n$	$P2_1/n$	$P2_1/c$	$C2/c$
a [Å]	11.9463(11)	12.065(2)	20.056(3)	11.734(17)
b [Å]	10.7375(10)	10.807(2)	14.147(2)	12.210(18)
c [Å]	13.6897(12)	14.208(3)	30.946(5)	8.893(13)
β [°]	107.5070(10)	107.441(2)	106.634(2)	98.457(12)
V [Å^3]	1674.7(3)	1767.4(6)	8413(2)	1260(3)
Z	4	4	24	4
ρ_{calcd} [g cm^{-3}]	1.317	1.455	1.440	1.471
F(000)	680	776	3696	568
Temperature [K]	100	100	100	100
Reflns collected	9139	9254	36973	2867
Independent reflns	3675	3855	13676	1114
Parameters	257	265	1057	84
R(int)	0.0145	0.0209	0.0322	0.1301
R_1[a], R_w[b] ($I > 2\sigma$)	0.0239, 0.0616	0.0410, 0.0957	0.0533, 0.1419	0.0455, 0.1189
R_1[a], R_w[b] (all data)	0.0246, 0.0628	0.0439, 0.0976	0.0603, 0.1455	0.0459, 0.1194
Goodness of fit	1.059	1.104	1.241	1.081
$\Delta\rho_{max,min}$ [e Å^{-3}]	0.322, –0.303	2.085, –0.833	2.573, –0.859	0.795, –0.867

[a] $R_1 = \Sigma||F_o| - |F_c|| / \Sigma|F_o|$. [b] $R_w = [\Sigma w (F_o^2 - F_c^2)^2 / \Sigma w (F_o^2)^2]^{1/2}$

Table S3. Crystallographic parameters

	[**1**][FAP]	[**2**][FAP]
Empirical formula	$C_{16}H_{10}F_{18}PCo$	$C_{17}H_{11}F_{18}PRu$
Formula weight	634.14	689.30
Crystal system	Monoclinic	Monoclinic
Space group	$P2_1/n$	$P2_1/n$
a [Å]	10.9470(9)	11.5747(10)
b [Å]	12.6504(10)	12.7379(11)
c [Å]	14.7816(12)	15.3578(14)
β [°]	98.0370(10)	101.0190(10)
V [Å^3]	2026.9(3)	2222.6(3)
Z	4	4
ρ_{calcd} [g cm^{-3}]	2.078	2.060
F(000)	1240	1336
Temperature [K]	100	100
Reflns collected	11163	10626
Independent reflns	4442	3926
Parameters	371	392
R(int)	0.0290	0.0224
$R_1{}^a$, $R_w{}^b$ ($I > 2\sigma$)	0.0267, 0.0697	0.0354, 0.0937
$R_1{}^a$, $R_w{}^b$ (all data)	0.0273, 0.0703	0.0391, 0.0985
Goodness of fit	1.102	1.043
$\Delta\rho_{max,min}$ [e Å^{-3}]	0.300, –0.674	0.686, –0.758

$^aR_1 = \Sigma||F_o| - |F_c|| / \Sigma|F_o|$. $^bR_w = [\Sigma w (F_o^2 - F_c^2)^2/\Sigma w (F_o^2)^2]^{1/2}$

Table S4. Crystallographic parameters

	[**2**][$CB_{11}H_{12}$]	[**2**][OTf]
Empirical formula	$C_{12}H_{23}B_{11}Ru$	$C_{12}H_{11}F_3O_3SRu$
Crystal system	Orthorhombic	Monoclinic
Space group	$Cmm2$	$P3_1$
a [Å]	10.1597(8)	10.205(2)
b [Å]	12.5270(10)	10.205(2)
c [Å]	7.2036(6)	10.868(2)
α [°]	90	90
β [°]	90	90
γ [°]	90	120
V [Å^3]	916.81(13)	980.2(4)
Temperature [K]	273	100